Powder Technology 485 (2027) 123140

Contents lists available at ScienceDirect

Powder Technology

journal homepage: www.journals.elsevier.com/powder-technology

Avalanches in disk-star mixtures in a slowly rotating quasi-two-dimensional drum

Francisco M. Díaz Torres [a], Luis A. Pugnaloni [a,c], Germán E. Varas Siriany [b],*

[a] Departamento de Física, Facultad de Ciencias Exactas y Naturales, Universidad Nacional de La Pampa, Uruguay 151, 6300 Santa Rosa (La Pampa), Argentina
[b] Instituto de Física, Pontificia Universidad Católica de Valparaíso (PUCV), Avenida Universidad 330, Valparaíso, Chile
[c] Consejo Nacional de Investigaciones Científicas y Técnicas, Buenos Aires, Argentina

GRAPHICAL ABSTRACT

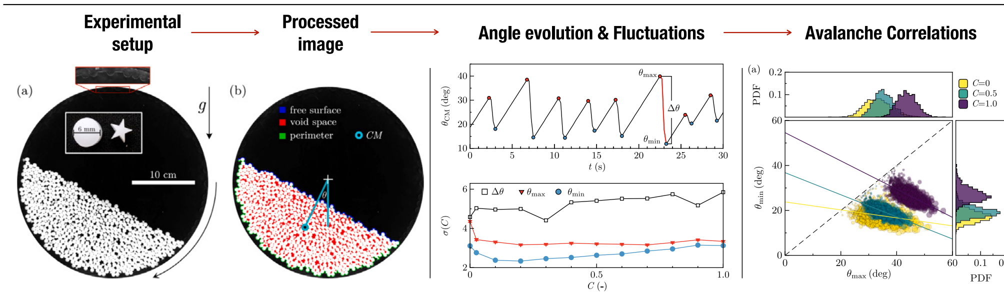

Conclusion

A small fraction of star-shaped grains strongly reduces fluctuations in the maximum angle of stability, while only weakly shifting its mean value.

HIGHLIGHTS

- Center-of-mass angle provides a robust avalanche descriptor and resolves micro-slips.
- A small fraction of star-shaped particles strongly suppresses avalanche fluctuations.
- Mean initiation and arrest angles remain positively correlated across mixtures.
- Event-by-event initiation and arrest angles show a systematic anticorrelation.

ARTICLE INFO

Keywords:
Granular intermittent flow
Particle shape effect
Binary mixtures

ABSTRACT

The mechanical response of mixtures of convex and non-convex particles has received less attention than mixtures of different convex shapes. We study the intermittent avalanches of a mixture of disks and five-pointed stars inside a quasi-two-dimensional slowly rotating drum. We consider mixtures where disks and stars have the same projected area (hence, the same mass) and mixtures where disks and stars have the same outer radius. We find that the equal-area condition leads to radial segregation, which hinders a clean interpretation of avalanche statistics. The equal-radius mixtures show no appreciable segregation within our metric. We consider a range of star fractions in the equal-radius mixtures. We find that even a small number of stars added to a disk sample can lead to significantly smaller fluctuations in the maximum angle of stability at which an avalanche is triggered. We show that, for a given composition, the maximum angle of stability is negatively correlated with the subsequent angle of repose (angle after avalanche relaxation). However,

* Corresponding author.
E-mail address: german.varas@pucv.cl (G.E.V. Siriany).

https://doi.org/10.1016/j.powtec.2026.123140
Received 28 April 2026; Received in revised form 3 August 2026; Accepted 20 August 2026
Available online 28 August 2026
0032-5910/

across compositions, the mean maximum angle of stability is positively correlated with the mean angle of repose, in agreement with previous studies on a range of granular materials. Because equal-radius disk-to-star substitution simultaneously changes particle shape, projected area, mass, bed filling, and internal packing, the observed reduction in fluctuations of the maximum stability angle cannot be uniquely attributed to particle non-convexity. These results nevertheless provide a reference for future studies in which these factors are independently controlled.

1. Introduction

The mechanical stability of a granular material is of great importance in industry, in civil engineering, and in mining [1]. This is so because of the need to store bulk materials in piles or silos, make them flow, and also dig in a granular material while avoiding avalanches. Although much has been investigated in this regard for rounded grains and also more complex convex shapes such as polygons (in two dimensions) and polyhedrons (in three dimensions), little is known about non-convex particles. Non-convex particles can more easily interlock [2] and even entangle [3,4], which leads to enhanced stability [2]. However, a number of challenges lie ahead when dealing with non-convex particles [5]. To mention one, a clear definition of shape parameters is non-trivial.

A standard stability test for granular materials is based on placing a sample of the material in a slowly rotating drum to assess the maximum angle of stability [6,7]. At moderate rotation speeds, the granular material flows continuously and develops a "dynamic" angle of repose that can characterize the flowability of the material. However, at very low speeds, the system flows intermittently (in avalanches) showing a maximum angle of stability and an angle of repose after each avalanche [7].

A number of studies have focused on characterizing materials other than disks and spheres using rotating drums. Piva et al. [8] have considered disks with a non-symmetric center of mass as well as disks with a movable center of mass. They show that particles made of a free body inside a hollow disk enhance the overall stability of the material whereas a non-symmetric center of mass reduces the stability. Cantelaube et al. [9] have studied convex pentagonal grains in two dimensions, which show a higher maximum angle of stability in comparison to disks. A study by Peng et al. [10] has considered not only spheres with different roughness but also bumpy grains. They have found that bumpy particles present higher angles of stability, in line with Cantelaube et al. but have also shown that these particles present larger fluctuations in the size of the avalanches in comparison to spheres. Interestingly, these authors have also demonstrated a correlation between the maximum angle of stability and the following angle of repose which is connected to inertial effects: a large angle at the beginning of the avalanche leads to a small repose angle. Höhner et al. [11] have modeled polyhedrons in a rotating drum but considered the dynamic angle of repose and mixing behavior rather than stability. In a related study, Chen et al. [12] have used the center of mass of the pack of non-spherical grains in a rotating drum instead of the angle of the free surface. Center-of-mass-based angle descriptors have also been used previously to characterize avalanching materials in rotating drums [13]. In the present work, we use the center-of-mass angle, θ_{CM}, as a practical descriptor of avalanche events. In the slowly driven regime studied here, where the free surface remains approximately straight, θ_{CM} provides a smooth signal for event detection while avoiding some ambiguities associated with fitting the free surface. Its usefulness, however, depends on the geometry and flow regime considered.

Only recently, some studies have focused on non-convex particles in a rotating drum. Preud'homme et al. [14] studied eight-pointed stars of varying sharpness. However, they performed experiments at moderate rotation speed to obtain the dynamic angle of repose. Wang et al. [15] run extensive simulations of non-convex particles in a drum, but with a focus on mixing behavior. A recent study also considers non-convex grains in a rotating drum, but then again in the regime of continuous flow [16].

In this work, we consider convex (disks) and non-convex (stars) grains in a two-dimensional slowly rotating drum operating in the intermittent-flow regime. We study the maximum angle of stability, the angle of repose, and the size of the avalanches, defined as the difference between these two angles. Unlike most previous works, we do not vary the shape of the particles to obtain different degrees of non-convexity. Instead, we consider binary mixtures of disks and stars to move from a purely convex (all disks) system to a purely non-convex (all stars) system. We first compare two protocols to match both particle species, namely equal projected area and equal outer radius. We show that the equal-area condition leads to radial segregation, which complicates the interpretation of avalanche statistics, whereas the equal-radius condition yields nearly homogeneous mixtures within our metric. We therefore focus on the latter case and study how avalanche statistics evolve with the fraction of stars. We find that the presence of a small number of stars, in a system mostly composed of disks, significantly alters the fluctuations in the maximum angle of stability.

2. Experimental setup

The experimental setup consists of a cylindrical drum with a circular PMMA base and lid (diameter $d = 292 \pm 1$ mm), separated by a spacer ring that sets the particle layer thickness [see Fig. 1(a)]. The ring has a thickness of 4.0 mm, equal to the particle thickness, ensuring that particles remain confined within the drum. To avoid jamming between the particle surfaces and the lids, small local spacers of 0.1 mm were distributed along the ring, creating a slight clearance that allows free particle motion. The inner edge of the ring has an irregular shape made out of small half-disks randomly spaced to prevent crystallization of the particles. The drum is filled with 700 laser-cut PMMA particles (static friction coefficient $\mu_{\text{static}} = 0.8$) of two characteristic shapes: disks and five-pointed stars. For both types, the characteristic size was set to $D = 6.0 \pm 0.1$ mm. For disks, D is the particle diameter; for stars, D is the diameter of the circumcircle that passes through the outer tips. The stars are also defined by an inner circle (3.0 mm in diameter) that forms the base for the limbs. Because the star occupies only a fraction of that circle, its projected area is smaller; accordingly, the particle areas are: $A_c \approx 28.3$ mm^2 for disks and $A_s \approx 10.1$ mm^2 for stars. In addition to the reference case with $N = 700$ particles, we also tested systems with different particle numbers to verify that the main avalanche statistics remain qualitatively robust with respect to filling fraction. Furthermore, we have tested systems in which the stars are scaled up to match the projected area, hence the mass, of the disks. Since the experiments use PMMA particles confined between PMMA plates, triboelectric charging cannot be completely excluded. However, our particles are millimetric ($D = 6$ mm and thickness 4 mm), whereas electrostatic effects in granular flows are typically more relevant for smaller particles, often below the millimeter scale, where aggregation or sticking to container walls may occur [17]. No persistent adhesion to the plates or long-lived aggregates were observed during the experiments.

The drum is mounted on two bearings to allow smooth rotation, driven by a motor coupled to its rear center. The motor includes an encoder to control the rotation speed (≈1.0 rpm). Each experiment is recorded for 90 min at 4 frames per second (fps) using a Basler

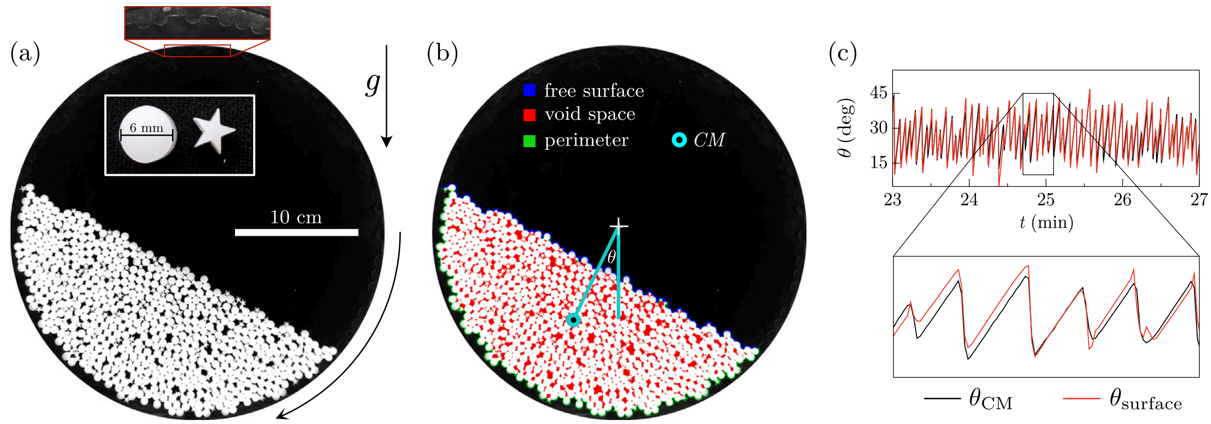

Fig. 1. Experimental setup. (a) Circular drum filled with a mixture of disks and star-shaped particles ($C = 0.2$). The inner edge of the spacer ring contains aperiodic roughness to prevent spontaneous crystallization at the boundaries. (b) Processed image of the system showing the free surface (blue), void space (red), particle perimeter (green), and the center of mass (cyan circle). The center-of-mass angle θ_{CM} is defined with respect to the vertical axis through the drum center. (c) Temporal evolution of the free-surface angle $\theta_{surface}$ (red line) and the center-of-mass angle θ_{CM} (black line). While $\theta_{surface}$ exhibits sharp spikes and stronger fluctuations, θ_{CM} provides a more stable measure of the system dynamics.

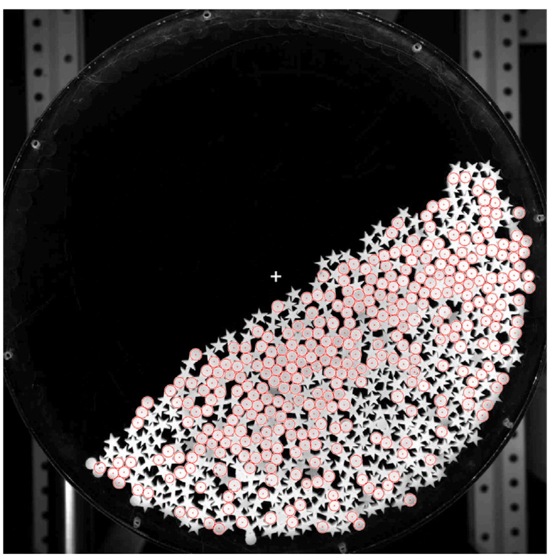

Fig. 2. Snapshot of the experiment with disks and stars of same area(mass) after 120 revolutions for $C = 0.5$. On visual inspection, clear segregation is observed with disks (highlighted in red) preferentially occupying the central region of the material. The red circles are shown only as a visual guide and may miss a few disks in individual frames.

a2A2840 camera (1420 × 1420 pixels). Before recording, the drum is left to rotate for several minutes to allow for any transient response to fade. The fraction of stars is quantified as $C = N_{stars}/(N_{stars} + N_{disks})$, with C ranging from 0 to 1. For each concentration C, we performed two independent 90-min recordings. Since the typical time between avalanches is 3–5 s, each concentration yields a large number of events; around 3000 detected avalanches were used in the statistical analysis.

Captured images are binarized (the threshold introduces an error of less than 1% in particle diameter) and processed using MATLAB®. From each frame, we extract the external perimeter, void space, free surface, and the center of mass of the granular assembly [Fig. 1(b)]. The free-surface angle, $\theta_{surface}$, is obtained by a linear fit to the coordinates of the particles located at the top layer [blue line in Fig. 1(b)], which defines the mean slope of the exposed surface. Unlike most studies, here we use the angle θ_{CM} defined by the vertical line that passes through the center of the drum and the line defined by the center of mass of the granular sample and the drum center, θ_{CM} [Fig. 1(b)]. At low rotation rates, the free surface is essentially straight and can be represented by a chord of the drum, which is perpendicular to the radius passing through the center of mass of the material. Consequently, the angle between the free surface and the horizontal is equivalent to the angle between that radius and the vertical. θ_{CM} provides a more robust measure than $\theta_{surface}$, as it does not depend on subtle details when defining the surface and is less sensitive to local fluctuations. As shown in Fig. 1(c), $\theta_{surface}$ exhibits some fluctuations before and/or after slips, whereas θ_{CM} evolves more smoothly over time.

The time resolution does not resolve the internal dynamics of individual avalanches, which last about 0.5 s. Therefore, our analysis is restricted to the pre- and post-avalanche states, rather than to the detailed dynamics during the avalanche. However, this frame rate is sufficient to capture the occurrence of each avalanche because the delay between successive events is long due to the slow rotation of the drum. In our case, the typical time between avalanches is about 5 s, corresponding to roughly 20 frames. At the imposed rotation rate of approximately 1 rpm, the drum advances about 6° per second, so the angular advance between two consecutive frames is about 1.5°. This value sets the angular scale associated with the frame-to-frame detection of the extrema. Similar low-frame-rate imaging has been used in slowly rotating drum experiments to extract global avalanche statistics [8].

3. Preliminary observations

3.1. Segregation

In order to consider systems where the two species of the mixture have the same projected area (and therefore the same mass), we run a series of experiments with mixtures of disks and stars of same area. Fig. 2 shows a sample image of such system for a $C = 0.5$ mix after 120 revolutions. As is apparent form the image, the system remains in a segregated state with the disks preferentially situated in the center of the material and the stars located in the surroundings. This segregation is observed for most experiments at various values of C. Segregation can obscure the analysis since it is not clear if a given effect can be attributed to the cooperation of the two types of particles or to the sole behavior of one of the species that occupies the free surface of the granular bed.

It is well known that in mixtures of rounded particles in a rotating drum small grains segregate to the central part of the bed [18]. This is explained by the fact that, in general, small particles will stop midway down the free surface in an avalanche trapped in the large irregularities

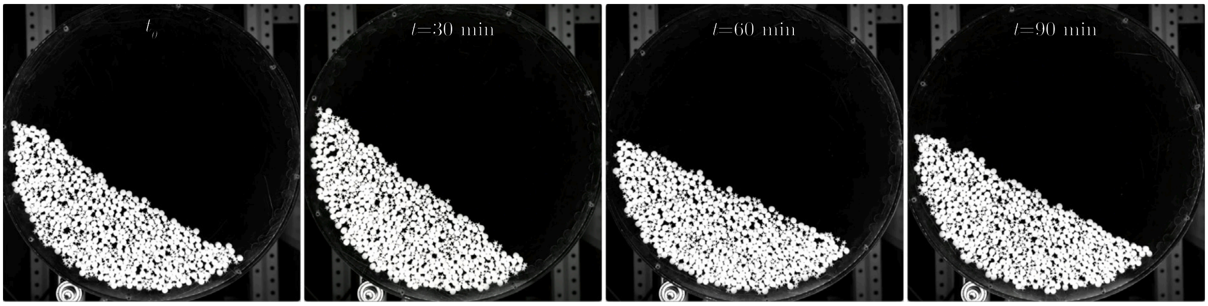

Fig. 3. Snapshots of the experiment at different times (Δt = 30 min, C = 0.5). The images show that, on visual inspection, no apparent segregation or large-scale rearrangement of the mixture can be observed during the experiment.

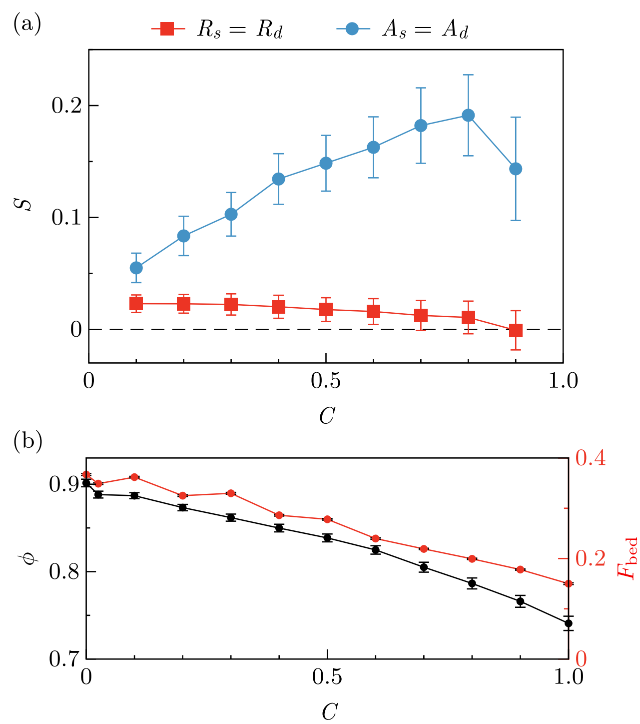

Fig. 4. (a) Segregation index S as a function of the star fraction C for stars with the same projected area as the disks ($A_s = A_d$, blue circles) and stars with the same outer radius ($R_s = R_d$, red squares). (b) Bed-area fraction $F_{\mathrm{bed}} = A_{\mathrm{group}}/A_{\mathrm{drum}}$ (red, right axis) and internal area packing fraction $\phi = A_p/A_{\mathrm{group}}$ (black, left axis) for the equal-radius mixtures. Here, A_p is the detected particle area and $A_{\mathrm{group}} = A_p + A_v$ is the measured area of the granular bed, including the detected internal voids.

created by the larger species. Hence, we expect that the tendency of the stars to roll far down the free surface and accumulate in the surroundings of the bed could be partially compensated by reducing their size. This would increase the probability of them getting trapped midway in a surface avalanche. We test this by using stars of same radius as the disks, which implied that stars have only 36% of the mass of a disk. Fig. 3 shows sample images for C = 0.5 at different times (t = 0, 30, 60, and 90 min) during the experiment. The overall distribution of particles remains visually homogeneous and no apparent segregation or systematic rearrangement is observed over the course of the experiment.

To quantify segregation we plot in Fig. 4(a) a segregation index S defined as $S = 1 - \langle r_{\mathrm{disks}}\rangle / \langle r_{\mathrm{stars}}\rangle$. Here, $\langle r\rangle$ is the mean distance of the disks(stars) to the center of the drum. We note that S is a global radial segregation index: it clearly distinguishes the strong radial segregation of the equal-area mixtures from the nearly homogeneous equal-radius mixtures, but it does not resolve possible local clustering or angular inhomogeneities. S tends to zero for a homogeneous mixture, is negative when stars concentrate in the central region and becomes positive when disks concentrate in the central region. As we can see, all mix ratios are nearly homogeneous for mixtures with small stars (same radius as the disks) but are clearly segregated with disks in the center ($S > 0$) for the large stars. This choice is a trade-off between the two protocols: equal-area mixtures keep particle mass fixed but segregate strongly, whereas equal-radius mixtures reduce radial segregation but change the projected area and mass of the stars, $m_s/m_d \simeq A_s/A_d \simeq 0.36$, as well as the local packing geometry. Thus, the results below should be interpreted as the avalanche response of a non-segregating disk–star mixture, not as a purely shape-controlled comparison. For the rest of the study we will focus only on the non-segregating systems of small stars.

For the equal-radius mixtures, we also quantified the two-dimensional filling level through the bed-area fraction $F_{\mathrm{bed}} = A_{\mathrm{group}}/A_{\mathrm{drum}}$, where $A_{\mathrm{group}} = A_{\mathrm{p}} + A_{\mathrm{v}}$ is the measured area of the granular bed (see Inset Fig. 4). We additionally calculated the internal area packing fraction, $\phi = A_{\mathrm{p}}/A_{\mathrm{group}}$. For the disk-only system, $\phi \simeq 0.90$, close to the ideal triangular-lattice packing fraction for monodisperse disks, $\phi_{\mathrm{hex}} = \pi/(2\sqrt{3}) \simeq 0.907$. As shown in Fig. 4(b), both quantities decrease overall as C increases: F_{bed} decreases from approximately 0.37 to 0.15, while ϕ decreases from approximately 0.90 to 0.74. Thus, replacing disks with equal-radius stars progressively reduces both the area occupied by the bed and the packing fraction within it.

3.2. Evolution of center of mass

The temporal evolution of the center-of-mass angle θ_{CM} is shown in Fig. 5(a). The signal alternates between two characteristic values: (i) the maximum angle of stability or avalanche angle θ_{max} (red dots), corresponding to the maximum slope of the free surface just before failure; and (ii) the repose angle θ_{min} (blue dots), the lowest slope reached once the avalanche stops. The avalanche size is quantified as the difference $\Delta\theta = \theta_{\mathrm{max}} - \theta_{\mathrm{min}}$.

In parallel, we extract the total particle area A_{p} [Fig. 5(b)] and the void area A_{v} [Fig. 5(c)]. For a given composition, A_p remains essentially constant in time, whereas A_v fluctuates due to particle rearrangements during avalanches. The mean value of A_p, however, varies across the concentration sweep because disks and equal-radius stars have different projected areas. This behavior reflects the classical Reynolds dilatancy effect: to enable flow, the packing must locally expand, which transiently increases A_{v} during avalanches. A minor detection loss of approximately ± 1 particle occurs during fast events, caused by motion blur that temporarily affects particle recognition. This loss has a negligible impact on the measured angles. Since we use the center-of-mass angle, missing one particle out of N = 700 represents a fractional mass error <0.2%. By contrast, surface-fitting methods rely on the ∼50–70 grains at the free surface — precisely the ones most affected by blur — so an equivalent single-particle loss would

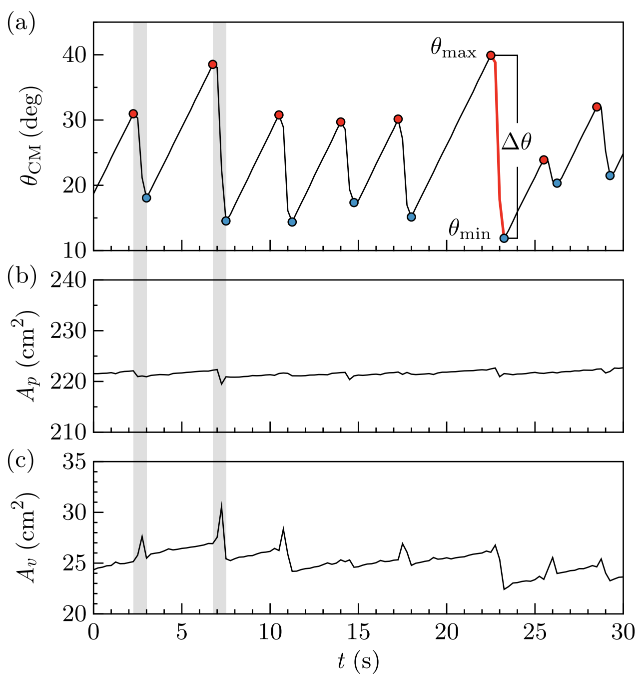

Fig. 5. (a) Evolution of the center-of-mass angle θ_{CM}. Peaks (red points) correspond to the avalanche angle θ_{max}, followed by minima (blue points) that define the repose angle θ_{min}. The difference between two consecutive extrema (red segment) defines the avalanche size $\Delta\theta$. (b) Evolution of the total particle area A_p, which remains nearly constant as the number of grains is fixed. (c) Evolution of the void area A_v, which fluctuates during avalanches. The gray transparent bar highlights the temporal correlation between drops in θ_{CM} and the corresponding fluctuations in A_v and A_p, marking the occurrence of avalanche events.

correspond to an effective sampling error of order 1/50–1/70 (∼1–2%), about an order of magnitude larger. This comparison supports the use of θ_{CM} as a practical and consistent event descriptor in the present experiments.

4. Results

In this section, we present results for the critical angle θ_{max} (Section 4.1), the repose angle θ_{min} (Section 4.2), and the avalanche amplitude $\Delta\theta$ (Section 4.3). Subsequently, we analyze the dispersion σ of these quantities as a function of concentration (Section 4.4), and finally we explore correlations between the characteristic angles (Section 4.5).

4.1. Critical angle θ_{max}

Fig. 6(a) shows the probability density functions of the maximum angle of stability θ_{max} for different proportions of star-shaped particles, each distribution centered by subtracting its mean value $\langle\theta_{max}\rangle$. In this representation, the curves collapse onto one another, indicating that the overall shape of the distributions is preserved across mixtures. The main visible difference is the width: the pure disk system (solid yellow circles) exhibits a significantly broader distribution, while the inclusion of even a small fraction of stars reduces the spread considerably.

These trends are summarized quantitatively in Fig. 6(b), which presents the data using boxplots. The median value of θ_{max} increases monotonically with the fraction of stars, from about 30° for pure disks up to 45° for pure stars. At the same time, the interquartile range, as well as the overall spread, decreases sharply once stars are introduced, confirming that the presence of angular particles homogenizes the avalanche onset. The combined analysis in Fig. 6 thus shows that while the mean stability grows steadily with the proportion of stars, the most

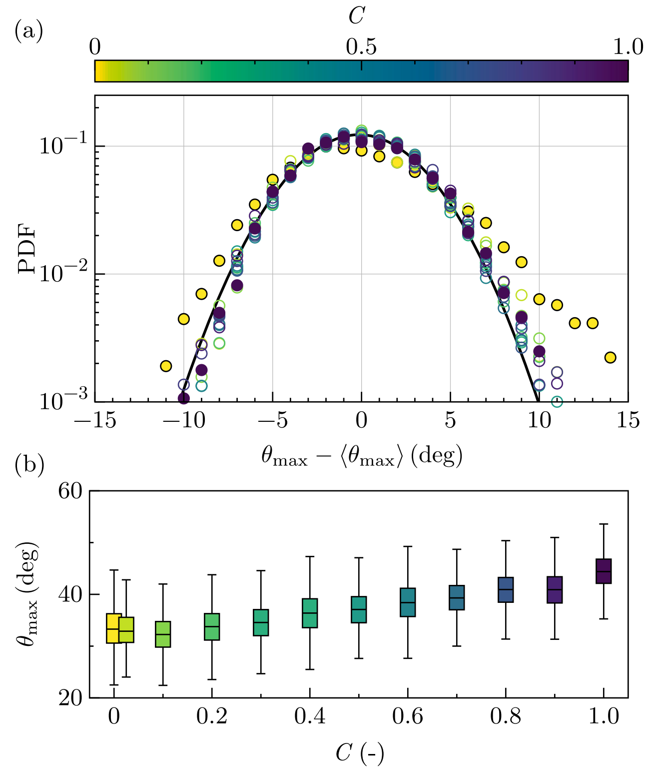

Fig. 6. (a) PDFs of θ_{max} for various values of C after subtracting the mean value $\langle\theta_{max}\rangle$ from each dataset. As the fraction of stars increases, the distributions shift to larger angles and become narrower. The pure disk system (solid yellow points) shows the broadest distribution, while the inclusion of even 2.5% of stars significantly reduces the spread. The solid blue points correspond to the pure star system and the solid line is a fit to a Gaussian distribution for the system with $C = 0.5$. (b) Boxplot representation of θ_{max} for different fractions of stars.

striking effect is the suppression of variability in θ_{max} once angular particles are present. This aspect will be further analyzed in Section 4.4, where all dispersions are compared as a function of concentration.

4.2. Angle of repose θ_{min}

After each avalanche, the final angle of repose θ_{min} is measured. Fig. 7(a) presents the PDFs of θ_{min} for different proportions of stars, while Fig. 7(b) shows the corresponding boxplots. In contrast to the case of θ_{max}, the PDFs of θ_{min} are clearly asymmetric: they display a pronounced tail towards large angles, indicating that the system can occasionally settle well above the mean. This asymmetry reveals that the relaxation after an avalanche is more variable and less constrained than the triggering of the avalanche itself. Such high repose angles suggest that the system can become trapped in metastable states arising from local packing heterogeneities and incomplete structural relaxation.

The mean values $\langle\theta_{min}\rangle$ increase smoothly with the fraction of stars, consistent with the stabilizing role of angular particles. Again, a detailed comparison of the dispersions as a function of C will be presented in Section 4.4.

4.3. Avalanche size $\Delta\theta$

The avalanche size, defined as $\Delta\theta = \theta_{max} - \theta_{min}$, quantifies the angular relaxation between the triggering and arrest of each avalanche. Physically, this parameter characterizes the angular relaxation of the bed and the extent of structural reorganization during the event. A direct energetic measure would require the vertical displacement of the

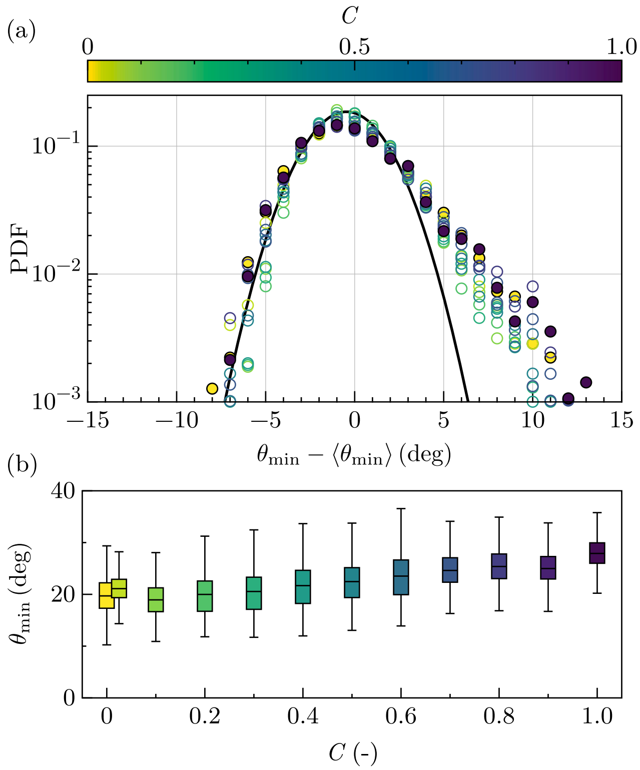

Fig. 7. (a) PDFs of $\theta_{\min}$ for various C after subtracting the mean value $\langle\theta_{\min}\rangle$ from each dataset. In contrast to $\theta_{\max}$, the distributions are asymmetric, with a pronounced tail towards angles above the mean, indicating a higher probability that avalanches stop above the mean. Solid yellow and solid blue symbols correspond to pure disk and pure star systems, respectively. The solid line is a Gaussian distribution to highlight the asymmetry of the PDFs. (b) Boxplot representation of $\theta_{\min}$ as a function of the star fraction C.

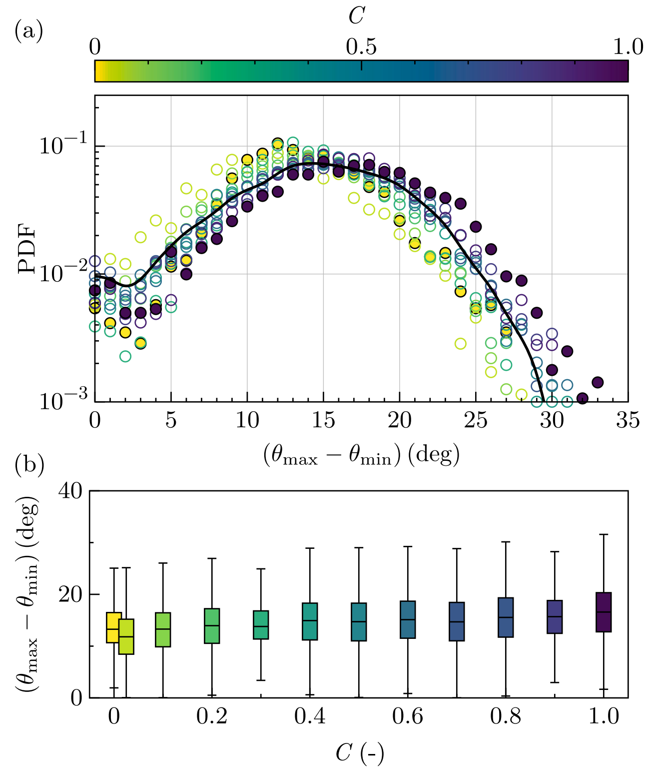

Fig. 8. (a) PDFs of $\Delta\theta$ for different fractions of stars. The black line serves as a visual guide. (b) Boxplot representation of $\Delta\theta$ as a function of the star fraction C.

center of mass, since $U = Mgy_{\mathrm{CM}}$. Here, $\Delta\theta$ is used as a geometric avalanche-size descriptor. Large values of $\Delta\theta$ correspond to system-spanning avalanches, while small values reflect local rearrangements or micro-slips.

The statistics of $\Delta\theta$ exhibit features distinct from those of $\theta_{\max}$ and $\theta_{\min}$ (see Fig. 8). A clear secondary peak emerges at very small $\Delta\theta$, corresponding to micro-slips or partial rearrangements of the packing. In contrast, the main peak at larger values ($\Delta\theta \approx 12°$) and the mean remain essentially invariant across mixture compositions. This invariance is confirmed by the boxplots in Fig. 8(b), which show that the median avalanche size does not vary significantly with C. A more detailed comparison of dispersions as a function of concentration will be presented in the following section.

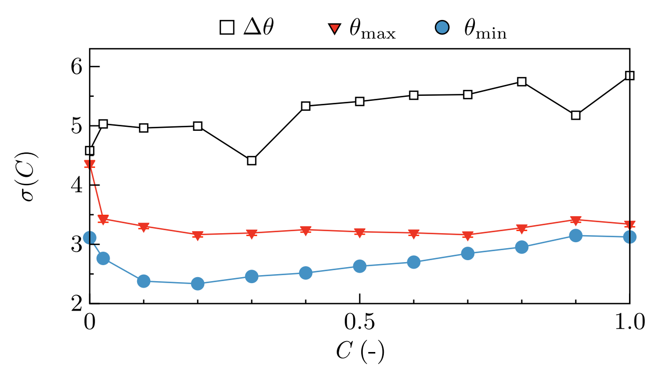

Fig. 9. Standard deviations of the avalanche angle $\theta_{\max}$, the repose angle $\theta_{\min}$, and the avalanche size $\Delta\theta$ as a function of the star concentration C. Error bars are smaller than the symbol size and therefore not visible.

4.4. Dispersion of avalanche angles

The standard deviations of $\theta_{\max}$, $\theta_{\min}$, and $\Delta\theta$ as functions of the star concentration C are shown in Fig. 9. A common trend is observed for $\theta_{\max}$ and $\theta_{\min}$: the introduction of a small fraction of stars into a disk-only system produces a sharp drop (>20%) in σ, indicating that the fluctuations of the avalanche dynamics become strongly reduced. This behavior shows that the addition of stars makes avalanche onset and arrest more reproducible, although it does not by itself identify the microscopic mechanism behind this stabilization.

Beyond the initial decrease, however, the dispersions evolve differently. For $\theta_{\min}$, σ grows steadily with C, eventually reaching values comparable to those of the pure-disk system. In contrast, for $\theta_{\max}$ the sharp initial drop is followed by a nearly constant dispersion, showing that the reproducibility of avalanche initiation remains robust once angular particles are present. For $\Delta\theta$, we observe an upward trend with increasing C albeit with small fluctuations along the curve.

The direct experimental result is the sharp reduction of the dispersion of $\theta_{\max}$ when stars are added. One possible interpretation is that avalanche onset changes from a response mainly controlled by local frictional yielding to one more constrained by geometry. In a pure disk system, failure is expected to depend on the contact network: force chains generate a broad distribution of normal forces [19], so different bed configurations may yield at different $\theta_{\max}$ values. In mixtures containing stars, local particle disentanglement may also be required before flow develops. This could make avalanche onset less sensitive to the particular force-chain configuration and more constrained by steric effects. This picture provides a possible physical interpretation of the observed narrowing of the $\theta_{\max}$ distribution, while a direct test

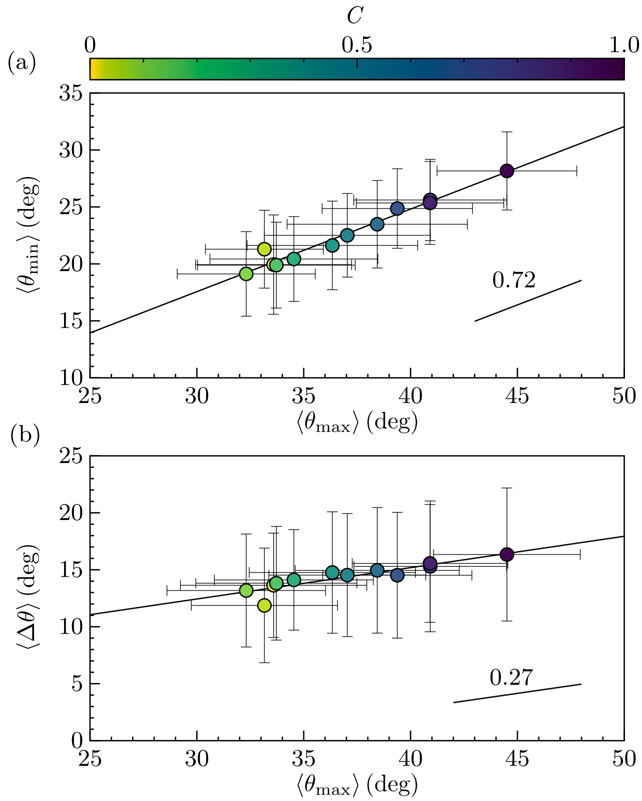

Fig. 10. Correlations between the mean values of characteristic avalanche angles for mixtures of disks and star-shaped particles. (a) Mean maximum angle of stability $\langle\theta_{\max}\rangle$ versus mean angle of repose $\langle\theta_{\min}\rangle$ for different star fractions C. The data follow an approximately linear trend, showing that the systems that are able to sustain larger inclinations before failure also relax into steeper repose states. (b) Mean maximum angle of stability $\langle\theta_{\max}\rangle$ versus mean avalanche size $\langle\Delta\theta\rangle$. A positive correlation is observed, indicating that systems that tend to trigger avalanches at higher $\theta_{\max}$ produce larger angular relaxations.

would require measurements of the contact network or particle-scale disentanglement.

In the present quasi-two-dimensional geometry, these steric effects may include both particle–particle and particle–wall contacts. Friction with the front and back confining plates is known to affect granular flows in rotating drums [20]. More generally, recent rotating-drum experiments have shown that drum width and lateral-wall effects can modify surface morphology and avalanche statistics [21]. In our setup, the flat particles remain parallel to the drum plane and a 0.1 mm clearance avoids particle trapping, so we do not expect a large permanent normal load against the front and back plates. Nevertheless, this clearance does not remove occasional particle–wall contacts or wall friction, especially during rearrangements and for star-shaped particles. Thus, the observed reduction in fluctuations should not be attributed only to particle–particle interlocking. We expect the same qualitative trend to persist in less-confined or fully three-dimensional systems, although with a weaker magnitude because out-of-plane rotations, tilting, and bypassing would provide additional relaxation mechanisms.

4.5. Correlations between characteristic angles

To explore couplings between the characteristic angles, Fig. 10(a) compares the means $\langle\theta_{\max}\rangle$ and $\langle\theta_{\min}\rangle$, and Fig. 10(b) with the mean avalanche size $\langle\Delta\theta\rangle$, for different star fractions C. In both cases, the data follow an approximately linear trend: systems that sustain, on average, larger inclinations before failure also tend to relax into steeper repose

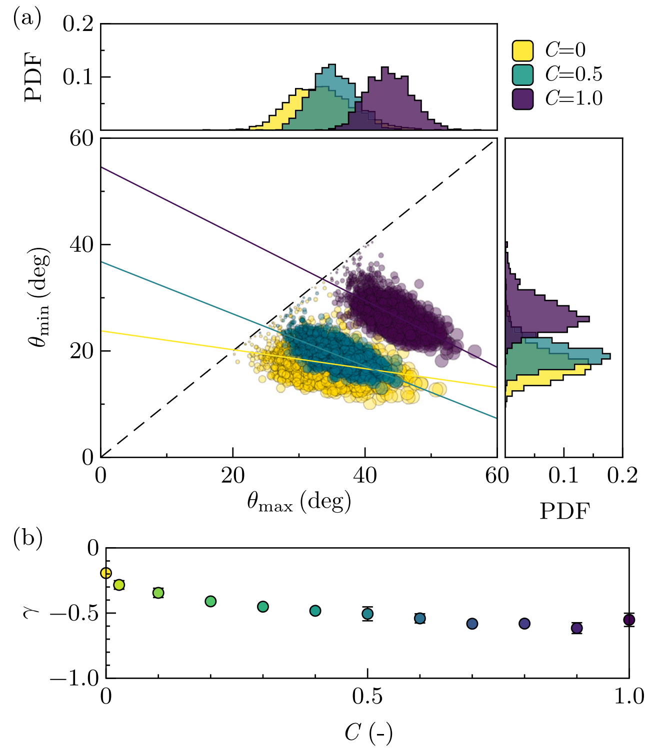

Fig. 11. (a) Correlation between the maximum angle of stability $\theta_{\max}$ and the subsequent repose angle $\theta_{\min}$ for each single avalanche in an experiment. Different star fractions C are represented with different colors (see legend). The avalanche size $\Delta\theta$ is represented by the size of the corresponding symbol. A negative correlation is observed, indicating that avalanches triggered at higher $\theta_{\max}$ tend to release more energy and result in larger slope drops. (b) Slope γ of the linear fit to the scatter plot in (a), shown as a function of star fraction C.

states and undergo larger slope drops. These correlations indicate that avalanche initiation and arrest, although distinct processes, are not fully independent. The same structural features that enable the system to resist higher inclinations — such as static friction and interlocking — also influence the final state after relaxation. In particular, the $\theta_{\max}$–$\theta_{\min}$ correlation supports the view that triggering and stopping are coupled stages of the avalanche process. A linear relation of the form,

$$\langle\theta_{\max}\rangle = \alpha\,\langle\theta_{\min}\rangle + \beta \tag{1}$$

has been reported in previous experiments with rotating drums [10,22], where it was shown to hold across particle types in the intermittent avalanche regime (low rotation speed). Our results corroborate this dependence, suggesting that the slope at failure statistically determines the residual stability after flow. In what follows, we focus only on the slope α, since the intercept β is not physically meaningful below the threshold angles ($\sim 15^\circ$) where avalanches do not occur. Recently, Liu et al. [22] found $\alpha \approx 0.65$ for a 3D drum and showed that this was in agreement with other experiments [22–24] where different granular materials are tested. Peng et al. [10] also reported a slope, which in our representation corresponds to $1/1.26 \approx 0.79$. We obtain $\alpha \approx 0.72$ for our 2D drum [see Fig. 10](a), a value that lies between the Liu and Peng estimates ($0.65 < 0.72 < 0.79$), and is thus consistent with both.

The $\theta_{\max}$–$\Delta\theta$ correlation shows that avalanches triggered at higher stability angles produce larger angular relaxations. This positive trend is consistent with previous observations in rotating drums and inclined-plane experiments [7,22,25], indicating that the onset angle statistically constrains the magnitude of the subsequent relaxation. Quantitatively, our fit yields a slope of $\alpha_{\Delta} \approx 0.27$, meaning that for each additional degree in $\theta_{\max}$ the avalanche size $\Delta\theta$ increases by about one quarter of a degree. This value is larger than the slope $\alpha_\Delta = 1/4.9 \approx 0.20$ reported by Peng et al. [10] for 3D drums. Although the numerical slopes differ, both experiments show the same positive relation between $\langle\Delta\theta\rangle$ and $\langle\theta_{\max}\rangle$. The difference may reflect the distinct experimental conditions, including dimensionality, particle properties, fitting procedure, and avalanche-detection method.

Beyond the correlation between mean values of the characteristic angles, one can survey the correlation between $\theta_{\max}$ and the following $\theta_{\min}$ for each single avalanche within a given experiment. This is done in Fig. 11(a) for the two pure systems and for an intermediate value of C. This correlation has been considered by others and a systematic negative slope, in agreement with our results, has been reported [24,26]. This negative correlation is caused by an inertial effect: avalanches that start at a higher angle have an initially higher potential energy to dissipate, which leads to a lower final repose angle. It is worth noting that the pure disk system presents a smaller slope (in absolute terms) than the mixtures with even a small fraction of stars. This implies that the inertial effect is more pronounced for systems containing non-convex particles. Fig. 11(b) summarizes these results by showing the slope γ of the linear fit as a function of C. This representation highlights that the anticorrelation is systematically stronger when non-convex particles are present. Fig. 11(a) also represents the size of each avalanche $\Delta\theta$ by the size of the corresponding symbol. As we can see, the presence of microslips (next to the dashed identity line) is well captured in this representation. Previous studies have underrepresented the existence of such micro-slips, likely due to the difficulties of capturing small rearrangements by fitting the free surface with a straight line, rather than considering the angle of the center of mass.

5. Conclusions

In this work, we characterized intermittent avalanches using the angle of the center of mass of the granular assembly. For the present slowly driven quasi-two-dimensional geometry, this descriptor provides a practical alternative to the free-surface angle, reducing the ambiguity associated with surface fitting and helping to identify small rearrangements.

Within this framework, we have shown that mixture composition affects avalanche initiation and arrest differently. The maximum angle of stability $\theta_{\max}$ responds strongly to equal-radius disk-to-star substitution: a very small fraction of stars mixed into a disk system can significantly diminish fluctuations, making avalanche triggering more reproducible while producing only a minor change in its mean value at low star fractions. Because equal-radius substitution simultaneously changes particle shape, projected area, mass, and packing geometry, the present experiments do not identify which of these factors controls the observed reduction in fluctuations. This reduced variability may nevertheless be relevant in applications where reproducible avalanche triggering is desirable. Future work should test whether this fluctuation reduction persists in fully three-dimensional systems, where out-of-plane rotations, tilting, and bypassing may modify the response to disk-to-star mixtures.

Finally, we observed that using star-shaped particles of same mass as the disks leads to a significant segregation in the system. In this case stars tend to locate at the periphery of the material. The change to use smaller stars, matching the radii rather than the area of the disks, allowed for a more homogeneous mixture. This approach may provide a useful starting point for future studies on controlled mixing and avalanche fluctuations. Future DEM simulations would be useful to disentangle these contributions by independently varying particle shape, projected area, mass, filling fraction, friction, wall interactions, and confinement, while monitoring the resulting packing structure.

CRediT authorship contribution statement

Francisco M. Díaz Torres: Methodology, Investigation, Data curation. **Luis A. Pugnaloni:** Writing – review & editing, Validation, Formal analysis, Conceptualization. **Germán E. Varas Siriany:** Writing – review & editing, Validation, Project administration, Formal analysis, Conceptualization.

Funding

This work was supported by UNLPam (grant F65) and Agencia Nacional de Investigación y Desarrollo (ANID, grant ID2310249).

Declaration of competing interest

The authors declare that they have no known competing financial interests or personal relationships that could have appeared to influence the work reported in this paper.

Acknowledgments

We thank Gino Sola (UNLPam) and Hans M. Adasme Villagrán (PUCV) for help with the experiments.

Data availability

Data will be made available on request.

References

[1] R.M. Nedderman, Statics and Kinematics of Granular Materials, Cambridge University Press, 1992.
[2] D.P. Huet, M. Jalaal, R. van Beek, D. van der Meer, A. Wachs, Granular avalanches of entangled rigid particles, Phys. Rev. Fluids 6 (10) (2021) 104304.
[3] N. Gravish, S.V. Franklin, D.L. Hu, D.I. Goldman, Entangled granular media, Phys. Rev. Lett. 108 (2012) 208001.
[4] Y. Zhao, K. Liu, M. Zheng, K. Dierichs J. Barés, A. Menges, R.P. Behringer, Packings of 3d stars: stability and structure, Granul. Matter 18 (2) (2016) 24.
[5] D. Cantor, M. Cárdenas-Barrantes, L.F. Orozco, Bespoke particle shapes in granular matter, Pap. Phys. 14 (2022) 140007.
[6] J. Duran, Sands, Powders, and Grains: An Introduction to the Physics of Granular Materials, Springer Science & Business Media, 2012.
[7] J. Rajchenbach, Flow in powders: From discrete avalanches to continuous regime, Phys. Rev. Lett. 65 (18) (1990) 2221.
[8] M. Piva, R.G. Martino, M.A. Aguirre J.-C. Géminard, Avalanches of grains with inhomogeneous distribution of inner mass, Phys. Rev. E 98 (6) (2018) 062902.
[9] F. Cantelaube, Y. Limon-Duparcmeur, D. Bideau, G. Ristow, Geometrical analysis of avalanches in a 2d drum, J. Phys. I 5 (5) (1995) 581–596.
[10] A. Peng, Y. Yuan, Y. Wang, Granular avalanche statistics in rotating drum with varied particle roughness, Natl. Sci. Open 2 (3) (2023) 20220069.
[11] D. Höhner, S. Wirtz, V. Scherer, A study on the influence of particle shape and shape approximation on particle mechanics in a rotating drum using the discrete element method, Powder Technol. 253 (2014) 256–265.
[12] J. Chen, D. Krengel, H.-G. Matuttis, Experimental Study of Particle Shape Dependence of Avalanches Inside a Rotating Drum, in: EPJ Web of Conferences, Vol. 249, EDP Sciences, 2021, p. 06001.
[13] M. Wojtkowski, O.I. Imole, M. Ramaioli, E. Chávez Montes, S. Luding, Behavior of cohesive powder in rotating drums, AIP Conf. Proc. 1542 (2013) 983–986, http://dx.doi.org/10.1063/1.4812098.
[14] E. Opsomer N. Preud'homme, N. Vandewalle, G. Lumay, Effect of Grain Shape on the Dynamics of Granular Materials in 2d Rotating Drum, in: EPJ Web of Conferences, Vol. 249, EDP Sciences, 2021, p. 06002.
[15] S. Wang, D. Liang, S. Ji, Dem study on mixing behaviors of concave-shaped particles in rotating drum based on level-set method, Powder Technol. 430 (2023) 118961.
[16] W. Wang, M. Renouf J. Barés, E. Azéma, Steady granular flow in a rotating drum: A theoretical nonlocal model for characterizing stress, velocity, and packing fraction profiles, encompassing grain shape effects from convex to highly concave, Phys. Rev. Res. 6 (4) (2024) 043310.
[17] N. Preud'homme, G. Lumay, N. Vandewalle, E. Opsomer, Tribocharging of granular materials and influence on their flow, Soft Matter 19 (2023) 8911–8918.

[18] J.M. Ottino, D.V. Khakhar, Mixing and segregation of granular materials, Annu. Rev. Fluid Mech. 32 (2000) 55.
[19] T.S. Majmudar, R.P. Behringer, Contact force measurements and stress-induced anisotropy in granular materials, Nature 435 (2005) 1079.
[20] N. Taberlet, P. Richard, E.J. Hinch, S shape of a granular pile in a rotating drum, Phys. Rev. E 73 (2006) 050301(R).
[21] A. Pol, R. Artoni, P. Richard, Cohesive granular material in a rotating drum: flow regimes and size effects, J. Fluid Mech. (2025) 1006.
[22] X.Y. Liu, E. Specht, J. Mellmann, Experimental study of the lower and upper angles of repose of granular materials in rotating drums, Powder Technol. 154 (2) (2005) 125–131.
[23] M.A. Carrigy, Experiments on the angles o f repose o f granular materials, Sedimentology 14 (1970) 147–158.
[24] N.J. Balmforth, J.N. McElwaine, From episodic avalanching to continuous flow in a granular drum, Granul. Matter 20 (3) (2018) 52.
[25] T. Börzsönyi, T.C. Halsey, R.E. Ecke, Avalanche dynamics on a rough inclined plane, Phys. Rev. E 78 (2008) 011306.
[26] R. Fischer, P. Gondret, B. Perrin, M. Rabaud, Dynamics of dry granular avalanches, Phys. Rev. E 78 (2008) 021302.